KLOE note n. 128
December 1994

High Precision Limited Streamer Drift Tubes

A. Calcaterra, R. de Sangro, G. Finocchiaro

INFN, Laboratori Nazionali di Frascati

ABSTRACT

A tracking telescope employing 6 layers of aluminum drift tubes 50 cm long, with diameter d=3 cm and wall thickness 500 μm, has been built and successfully operated with a $40\%\mathrm{Ar} - 60\% i\mathrm{C_4H_{10}}$ gas mixture at atmospheric pressure. The tube cells, with a 100 μm thick Cu-Be wire strung along the axis, enter streamer mode operation at V=4.6 kV, featuring full efficiency and local resolution of $\leq 60\,\mu$m.

1. Introduction

The device described here has been conceived and built, on the basis of past experience with ordinary plastic limited streamer tubes, to provide one of the two separate external reference trackers needed to study the performances of a small prototype of the main drift chamber of the KLOE detector. In the present note we present results obtained with the data that were taken in September 94 at the X7 test beam area of the CERN-SPS whith the main purpose of studying the KLOE drift chamber prototype. Although a complete description of the prototype (prototype 0.3), the external trackers, the test set-up and a more detailed discussion of the goals and results of the test will be the subject of a forthcoming comprehensive paper, we felt that the excellent tracking performances that have been achieved with the telescope described in the following deserved a dedicated discussion.

2. Mechanical Construction

Two identical trackers (mini-trackers, MT in the following) sandwiched around prototype 0.3 (see fig. 1), form the telescope. Each MT is made of 3 layers of 9+8+9 tubes; the central layer is vertically offset with respect to the inner and outer ones by one tube radius (1.5 cm), and the horizontal distance between layers is 4 cm. The aluminum tubes are cut to the final length from selected ~ 6 m long tubes. To reduce the chance of electrostatic discharge at the high operating voltage of the streamer regime, the tube inner surfaces have been polished. To facilitate the tight assembly of the almost-hexagonal structure, we have polished also the outer surface.

The outer frame, also made of aluminum, has been machined on a digitally controlled mill, ensuring mechanical positioning at the level of $\leq 30\,\mu$m. The two endplates of each tracker carry the 26 holes for the *delrin* wire feed-throughs which are concentric to 26 cylindrical pits that house and hold the aluminum tubes in their nominal position: the diaphragms separating adjacent pits have a thickness of $100\,\mu$m. At the bottom of the pits, a cylindrical groove having a $2{\times}2\,\mathrm{mm}^2$ section was machined all around their inner circumpherence, see fig. 2. A slow-hardening, non-running glue fills the grooves providing mechanical strength and excellent gas tightness.

We drilled another set of holes parallel to the feed-through holes and as close as possible to the outer radius of the tubes to accomodate small diameter, fast-on gas connectors [2]. Because these have a metal nut, a spark could occur if they were too close to the HV pins.

The tubes are glued onto the frame at both ends simultaneously. The process is delicate due to the necessity of respecting the thin diaphragms between adjacent pits, and took ~ 2 hours for each MT to complete. The frame is mounted and tightened with bolts at the same time.

The geometric precision and repeatability of the frame assembly are ensured by a number of precision positioning dowel pins. Other dowel pins are used to mount the two mini-trackers onto the KLOE prototype, whose external frame has also been machined on a numeric mill.

After allowing 48 hours for glue hardening, we strung 100 μm thick Cu-Be wires through the feed-through holes, soldered them at one end, tensioned them at 150 g and finally soldered the other end.

The 26 tubes in each MT were connected together with a daisy-chain of 4 mm diameter gas tubes, which we bent to a small radius using a hot-air gun.

3. Streamer mode operation

We chose to operate the tubes with a gas mixture of $40\%\mathrm{Ar}-60\% i\mathrm{C_4H_{10}}$ in the limited streamer regime to take advantage of the very large signals: first they do not need any preamplification before the discrimination, which increases the simplicity and reduces the cost of the read-out electronics; secondly the very high signal-to-noise ratio reduces the effect of the time jitter and improves the resolution of the drift distance measurement.

A picture of a typical streamer signal as seen with an oscilloscope is shown in fig. 3. One can see that indeed the pulse height is $\sim$ 400-500 mV over 50 Ω when the device is operated at 5.7 kV, and the signals have the characteristic $\sim$ 100 ns duration of a streamer.

The tubes enter the limited streamer mode of operation at a voltage of $\sim$ 4.6 kV and show a very long efficiency plateau (fig. 4). The curve has been obtained with a discrimination threshold of 15 mV.

We operated the tubes at a voltage of 5.7 kV, that is almost 1000 V (instead of the usual $\sim$ 100 V) above the plateau knee. The reason for having such a high electric field in the tubes was both to have longer streamers (and therefore higher signals) and to increase the drift velocity away from the wire.

It is well known that one of the characteristics of the streamer discharge is to produce a high number of UV photons, some of which may occasionally reach the cathod thereby extracting electrons. This effect is very pronounced when the cathode material is aluminum, as in our case, because of its low work function ($\sim$ 2.98 eV). These electrons may cause a second streamer to occur after the first one, with a delay given by their drift time from the cathode to the wire ($\sim$ 300 ns in our case). The probability of having after pulses increases with the operating voltage; since all the after-pulses are streamers themselves, and all streamers produce almost the same signal, all the afterpulses signals are as high as the first one. An example of this behaviour is shown in fig. 3, where oscilloscope signals for an operating voltage of 5.7 kV are shown and it is evident the $\sim$ 300 ns delay between afterpulses.

To have an idea of the probability of having 1, 2, 3 etc. afterpulses, we have used a digital oscilloscope to obtain the picture shown in fig. 5 which represent the average of 1000 events. The oscilloscope was triggered on the first streamer. Since the after-pulses are all of about the same height, and occur always with the same delay with respect to the first one, the relative height of the different peaks to the height of the first one reflects the number of times each after-pulse occurred over the 1000 triggers. One can see that, operating at 5.7 kV, 2/3 of the times one afterpulse is present, 1/2 of the times there are two, and as many as 6 or 7 but with much less probability. At lower operating voltage, the number of afterpulses is lower.

The presence of afterpulses does not pose any problem for our application where we are interested only in the time of arrival of the first pulse, which measures the drift distance of the closest ionization cluster left by the particles traversing the tubes. To reduce the probability of discriminator retriggering, we set the discriminator output gate to 2 μs, a time during which the discriminator was inhibited. The plateau curves shown in fig. 4 were indeed made with three different gate durations, 200 ns, 400 ns and 2 μs. With the longest gate the plateau extends to 6.0 kV because the afterpulsing could not contribute to the counting rate (at least up to events with ≤ 7 afterpulses, which we have already shown to be very few). The rate was of course well below the limit introduced by the 2 μs dead time, and the very long plateau is therefore an indication of the absence of noise or discharging. The tubes worked well up to 6 kV.

The high number of afterpulses does increase the total integrated charge on the wires for a given time of operation. This could lead to a faster ageing of the device; a study of this aspect has just begun, and we do not have any data at present. In fig. 6 we show the charge collected on the wires as a function of the operating voltage for data taken with cosmic rays.

The intrinsic recovery time of the device is the duration of the streamer pulse ($\sim$ 100 ns); to this one must add the maximum drift time, that in our case was $\leq$ 300 ns. The maximum rate that the device can withstand depends also on the number of afterpulses present at the chosen operating voltage. In our case (2 μs gate) it was limited to 500 kHz.

4. Test Setup

The KLOE chamber prototype with attached the two MT's was put in the X7 beam test area of the CERN SPS and exposed to a beam of 50 GeV pions.

The trigger was provided by the coincidence of two scintillators; this signal was used to start the 12 bit, 125 ps/channel CAMAC TDC's and was affected by a very small ($\leq$ 300 ps) time jitter.

The signals from the MT's were discriminated with a 15 mV threshold, delayed and sent to the TDC stops.

5. Drift Velocity and Local Resolution

Knowledge and use of the appropriate space-time relation is a major ingredient needed to obtain a good spatial resolution. Neglecting displacements of the wires and imperfections in the manufacturing of the tubes, the electric field in our devices has the simple behaviour $E = \kappa/r$, with $\kappa = 999\,\mathrm{V}$ @ $5.7\,\mathrm{kV}$. A typical time spectrum at this operating voltage is shown in fig. 7. The end point around 300 ns indicates for our 1.5 cm tubes an average mean drift velocity of $\sim 50\,\mu\mathrm{m/ns}$, as is expected for typical argon-isobutane mixtures [1] at these electric field values; the distribution also shows that the drift velocity is not saturated, otherwise it would be flat, given the fact that the illumination of the tube was reasonably uniform.

That the drift velocity is not constant is also apparent in the plot shown in fig. 8, which shows the correlation $t_{\mathrm{stag}} = (t_1 + t_3)/2 + t_2$ as a function of t_2, in three adjacent tubes belonging to the same mini tracker. The geometry of the tube triplet and the symbols are illustrated in fig. 9. Here again one would expect a flat t_{stag} for a saturated drift velocity, since this combination of times adds up to the total drift time corresponding to the stagger between the tubes which is 1.505 cm.

From the plot in fig. 8 we can obtain the spatial resolution of the device: the fluctuations around the mean value of t_{stag} are indeed a measurement of the convolved resolutions of the three tubes. The resolution of the single tube is therefore given by $\sigma = \sqrt{2/3} \times \sigma_{\mathrm{stag}}$, when one neglects the dependence of the spatial resolution from the drift distance. This last assumption will be shown to be essentially correct in the following.

According to a more refined description, the drift velocity is parametrised as $v_{\mathrm{drift}} \equiv \mu E = mE/(aE + 1)$ [3], where μ represents the electron mobility in the gas. This corresponds to a quadratic space-time relation in the tubes: $t = t_0 + Ax^2 + B|x|$, x being the drift distance.

In order to determine the coefficients A and B for the equation above, we have used the definition of x_{stag}, fitting it to its nominal value 1.505 cm. The use of the quadratic space-time relation with coefficients fitted in this way, produced a distribution which was flat at the $\simeq 75\,\mu\mathrm{m}$ level (fig. 10).

To correct these residual effects, we decided to study in more detail the space-time relation to be used in the tubes.

To solve the transport equations for the electron drift in the $40\%\mathrm{Ar} - 60\% i\mathrm{C_4H_{10}}$ gas mixture we used the computer code `MAGBOLTZ` [4] as implemented in the `GARFIELD` [5] program. The result of the study is shown in Fig. 11, where the drift velocity is plotted as a function of the distance from the sense wire. We observe that the parabolic approximation is valid only for drift distances $\gtrsim 0.5\,\mathrm{cm}$, as the coefficients A and B describing v_{drift} in such a region are in remarkably good agreement with the ones fitted from our data. For higher electric fields v_{drift} is seen first to decrease slightly, then to increase to very high values. This behaviour is apparent also from the time spectrum of the tubes shown in fig. 7, which corresponds, when the tube is uniformly illuminated, to the spectrum of drift velocity.

We defined a 7-parameter function, which is shown superimposed on the points from the MAGBOLTZ simulation in fig. 11. With this function we re-fit our data: the result of the minimization of x_{stag} is shown in fig. 12: the residuals are now almost free of any dependence on the drift distance, making the spatial resolution averaged over the whole tube almost as good as the local one ($\simeq 65\,\mu$m).

We can conclude that starting from the 'theoretical' input of MAGBOLTZ+GARFIELD, which make use of the measured electron cross sections, we have found a parametrization for the space-time relation, which can describe our data very well. We realized however that, from the practical point of view, a much simpler function could be used to parametrise the data, with very little loss of spatial resolution. This function is a parabola for $|x| \geq x_{\mathrm{cut}}$, which turns into a straight line (saturated drift velocity) for shorter drift distances. The slope of the straight line results from an average over the (small) region (closer to the wire) of very high drift velocity and the more extended (between 1 and 5 mm) region of slightly lower drift velocity. x_{cut} together with the three free parameters of this new function are again determined from a fit to the function x_{stag}. We have fitted the space-time relation in various tube triplets and verified that the fit parameters varied only a few percent from each other, and basically were the same within the errors. In the track fit (see next section) we have used only one set of space-time relation parameters for all the tubes.

6. Efficiency and Global Resolution

After determining the space-time relation to be used in the tubes, we have studied their performances as trackers. The distribution of the hit tubes is shown in fig. 13. The most probable value is 6: the small tails to lower values are mostly due to the dead space introduced by the 500 μm-thick aluminum walls. This result indicates already a high tube efficiency. To produce this plot a hit was defined as a tube whose corresponding TDC reading gave a signal which translated into a drift distance smaller than a tube radius. The tube efficiency shown in fig. 14 however, was calculated requiring also a consistency between the expected drift time of the track and the drift time actually measured in the tube. The expected drift time was obtained from the measurement of the tubes in the layer in front (t_1) and behind (t_3) the tube: $(t_1+t_3)/2 = t_{\mathrm{max}} - t_2$, t_2 being the measurement in the tube whose efficiency we are measuring, and t_{max} the maximum drift time. As this plot shows, an efficiency of $\geq 97\%$ is found at the tube border, and closer to 100% elsewere.

In fig. 15 the residuals from a straight-line fit to the selected hits are shown, as a function of the distance from the corresponding sense wires, for tubes belonging to different columns in the MT structure, and in fig. 16 their projection over the entire tube. Given the fact that the tubes were included in the fit, to obtain the true widths one must divide the observed ones by coefficients (respectively 0.781, 0.818 and 0.848 for tubes belonging to the outer, central and inner column of each MT) of easy derivation from the formulae of linear least-square fits. The single wire resolution is therefore $\sim 60\,\mu$m, with deviations of $\leq \pm 10\,\mu$m from tube to tube.

In fig. 17 the χ^2 of the fit in the cases when all six tubes were hit is shown; the distribution, obtained assigning an error of $70\,\mu$m to the individual tubes, is in turn fitted with a χ^2 function with 4 degrees of freedom. The corresponding probability distribution is compared in fig. 18 with the analogous ones in the case when an error of 60 and $80\,\mu$m, respectively, is assigned to the individual measurements. It is seen that $70\,\mu$m makes the $Prob(\chi^2)$ distribution flat. This value is slightly worse than the error in the single tube, a difference which we attribute mainly to the displacements ($\mathcal{O}(30 \div 50\,\mu\text{m})$) of the wires with respect to their nominal positions.

We have also operated the MT's at different high voltage values. In fig. 19 we show the resolution as a function of the drift distance for runs taken at 5.1, 5.4 and 6.0 kV compared to the one at 5.7 kV. We observed no degradation in the resolution of the device even when running at the lowest high voltage value, where the number of afterpulses is significantly reduced and therefore the device can sustain much higher single counting rates. Also the efficiency for these runs has been calculated, and is shown in fig. 20. There is no significant loss in the efficiency even operating at 5.1 kV.

As a last remark, we want to stress the importance of a careful evaluation of the t_0's for each individual channel, since an error in the t_0 determination reflects in double peaks in the distributions of the residuals. Also important in our opinion is the fact that we have used *the same* coefficients for the space-time relation in all the tubes.

7. Operation in a Magnetic Field

While the results discussed so far refer to the operation in absence of magnetic field, a number of runs were taken with the device immersed in a magnetic field of 0.6 Tesla directed parallel to the wires. We did not perform a complete analysis of these data, but preliminary results are shown in in fig. 21, where we plot the distribution of t_{stag} as a function the drift distance and its projection over the whole cell. One can see that there is a little deterioration in the global resolution. The space-time relation was fitted with the parabola+straight line, but without all the refined corrections on the t_0's, TDC calibrations, etc., which were made for the runs without the magnetic field. The work is still in progress to complete the magnetic field data analysis.

8. Further Developments

One major question on the operation of the device is the stability of its performances over time, question that arises given the significant amount of charge that is produced in the high gas amplification regime of operation. We are planning to make a study of the long term behaviour of this tubes.

Also, one should check whether the streamer mode of operation is compatible with its use in high radiation environment, such as that of the LHC.

ACKNOWLEDGMENTS

We would like to thank all the people of the KLOE drift chamber group who partecipated in the proto 0.3 test beam at CERN. They made a smooth and successful data taking possible. A special thank to dr. L. Pontecorvo for providing us with the aluminum tubes that were used to make the MT's and for his help in many "emergency" situations during the test beam. We would also like to thank E. Iannotti, without whose technical skills and dedication the MT would have never been built on time for the test beam, and to S. Di Virgilio for making the scintillator counters.

REFERENCES

1. F. Sauli, *Yellow Report*, CERN 77-09 (1977).
2. O.T.I. ROMA S.r.l. - Rome, Italy.
3. P.Santantonio, *A parametrization of the electron mobility in a helium based gas mixture*, KLOE note n. 77/93 (December 1993).
4. S.Biagi, *NIM* **A283**, 716 (1989).
5. R.Veenhof, *Garfield, a drift-chamber simulation program*, CERN program library (entry W5050).

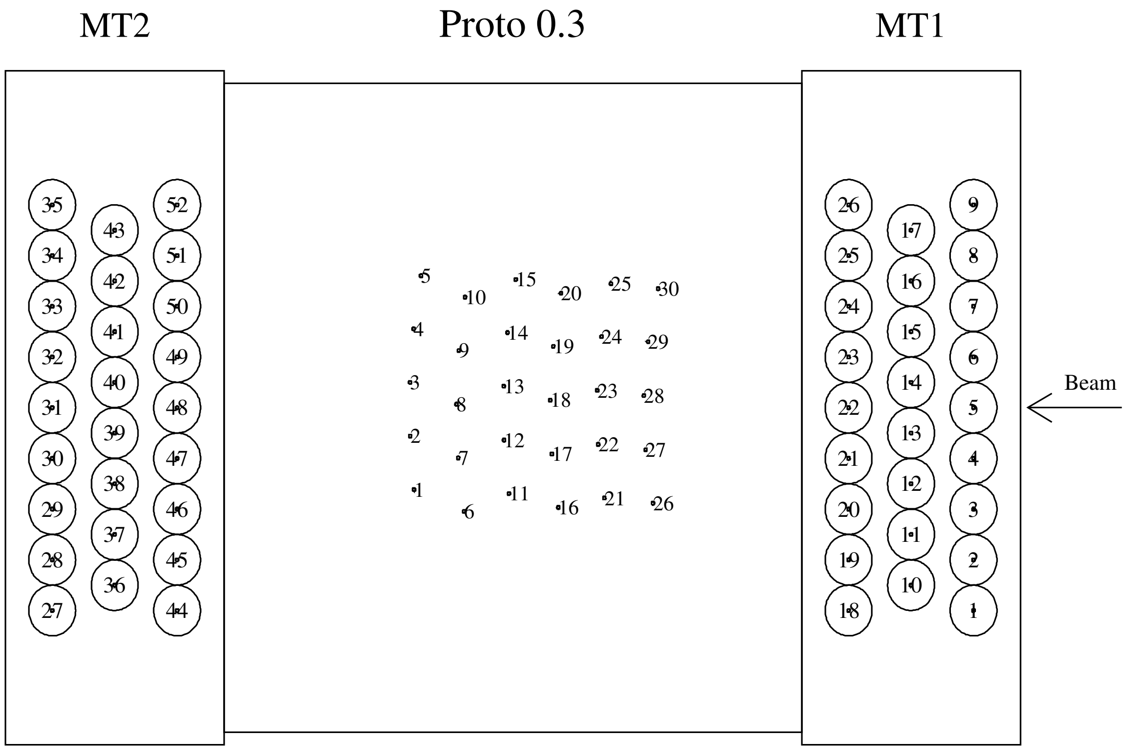

Fig. 1: *Sketch of the setup used at the CERN test.*

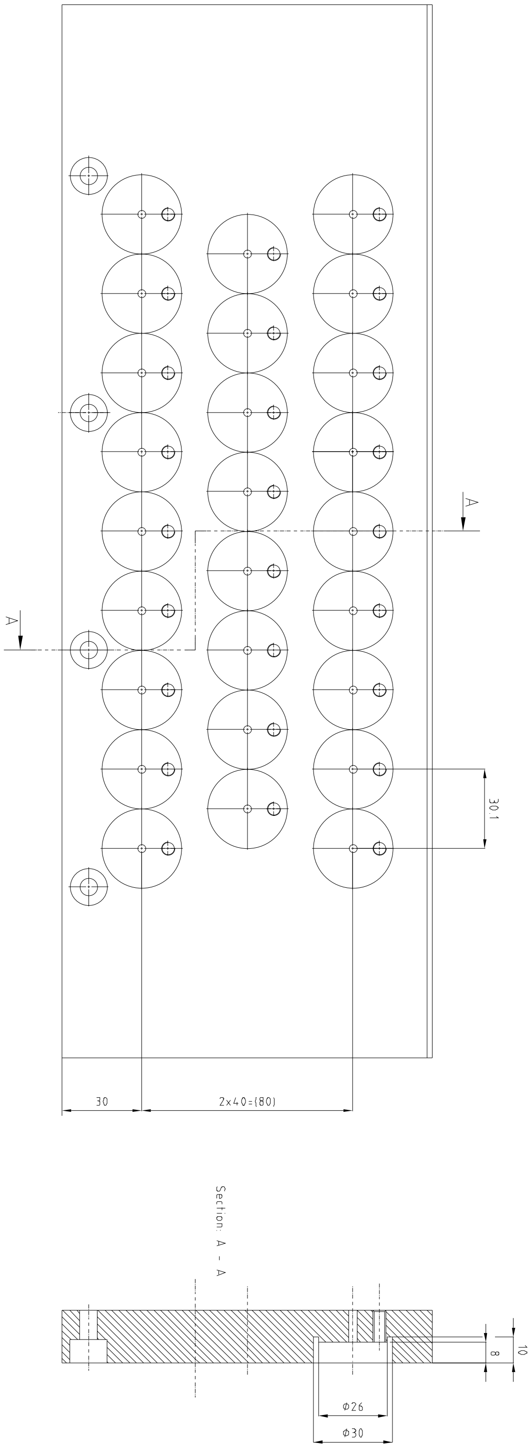

Fig. 2: *Mechanical drawing showing the details of the end plate design.*

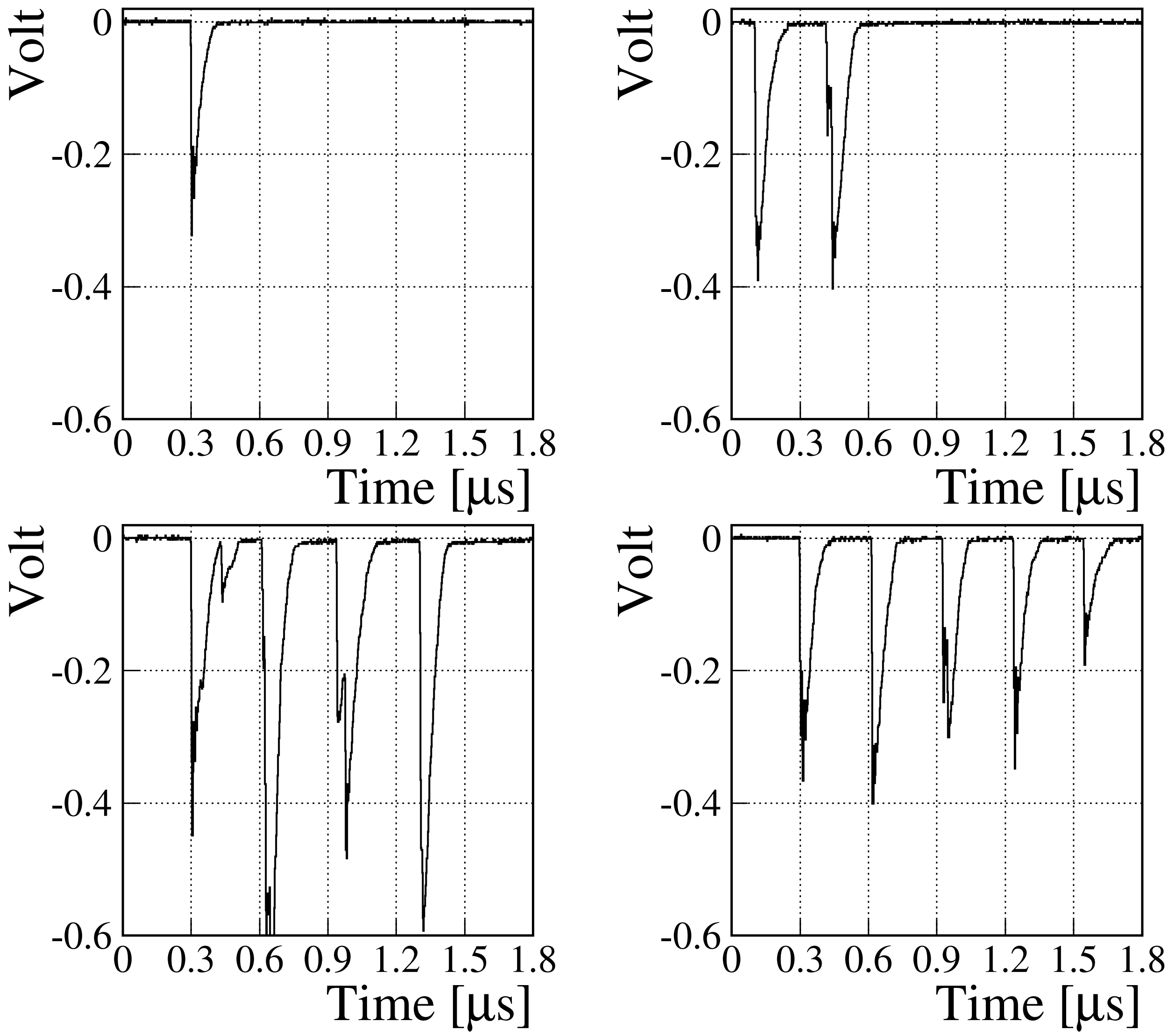

Fig. 3: *Example of streamer signals on an oscilloscope terminated on 50 Ω. The pictures were all taken at 5.7* kV.

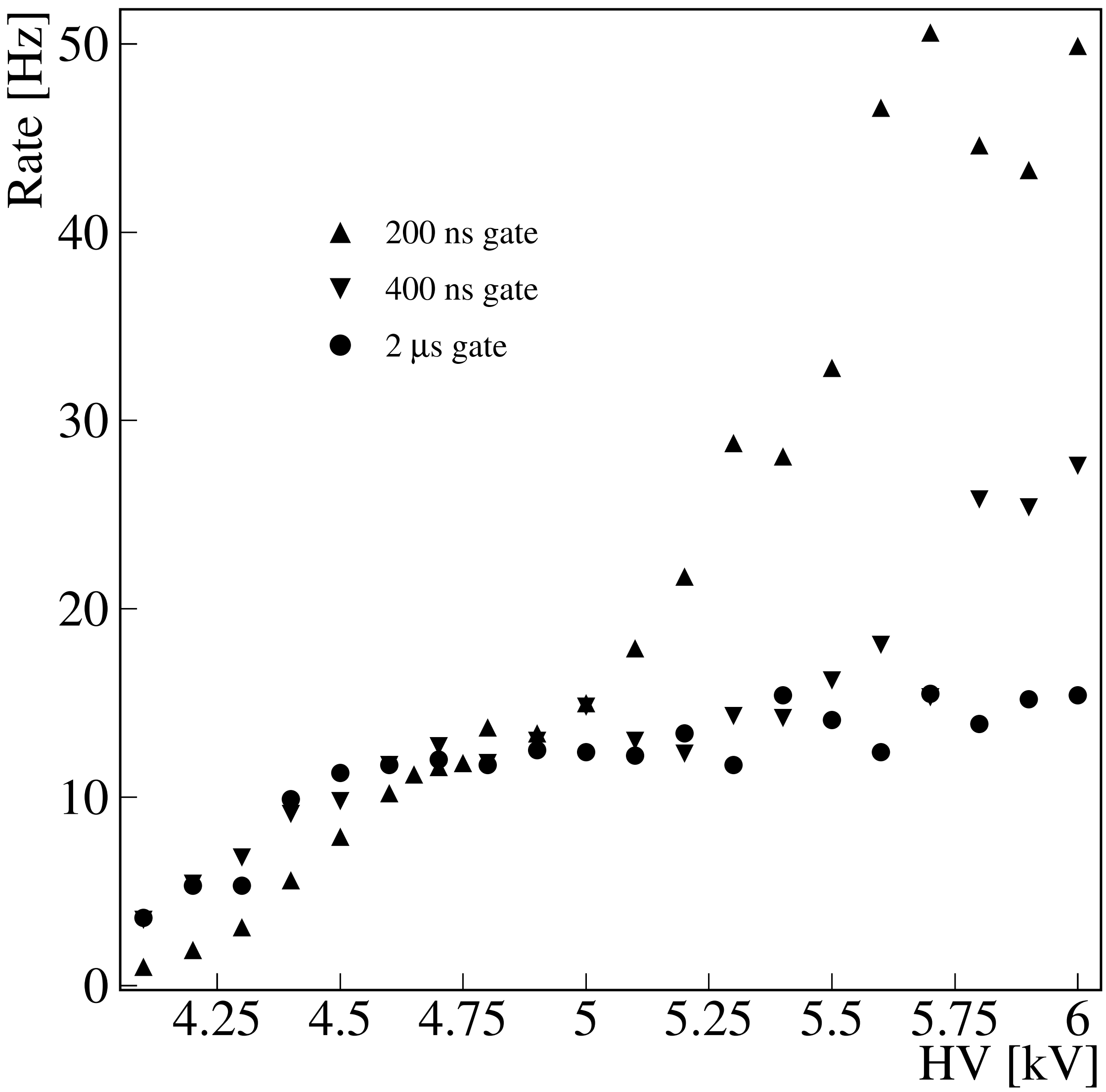

Fig. 4: *Singles plateau curves obtained with 200*ns, *400*ns *and 2*μs *gates. For the curve with the gate at 200*ns *the signals were attenuated by 4db, but were discriminated with the same threshold, which explains why the counting rate is lower until it reaches the plateau.*

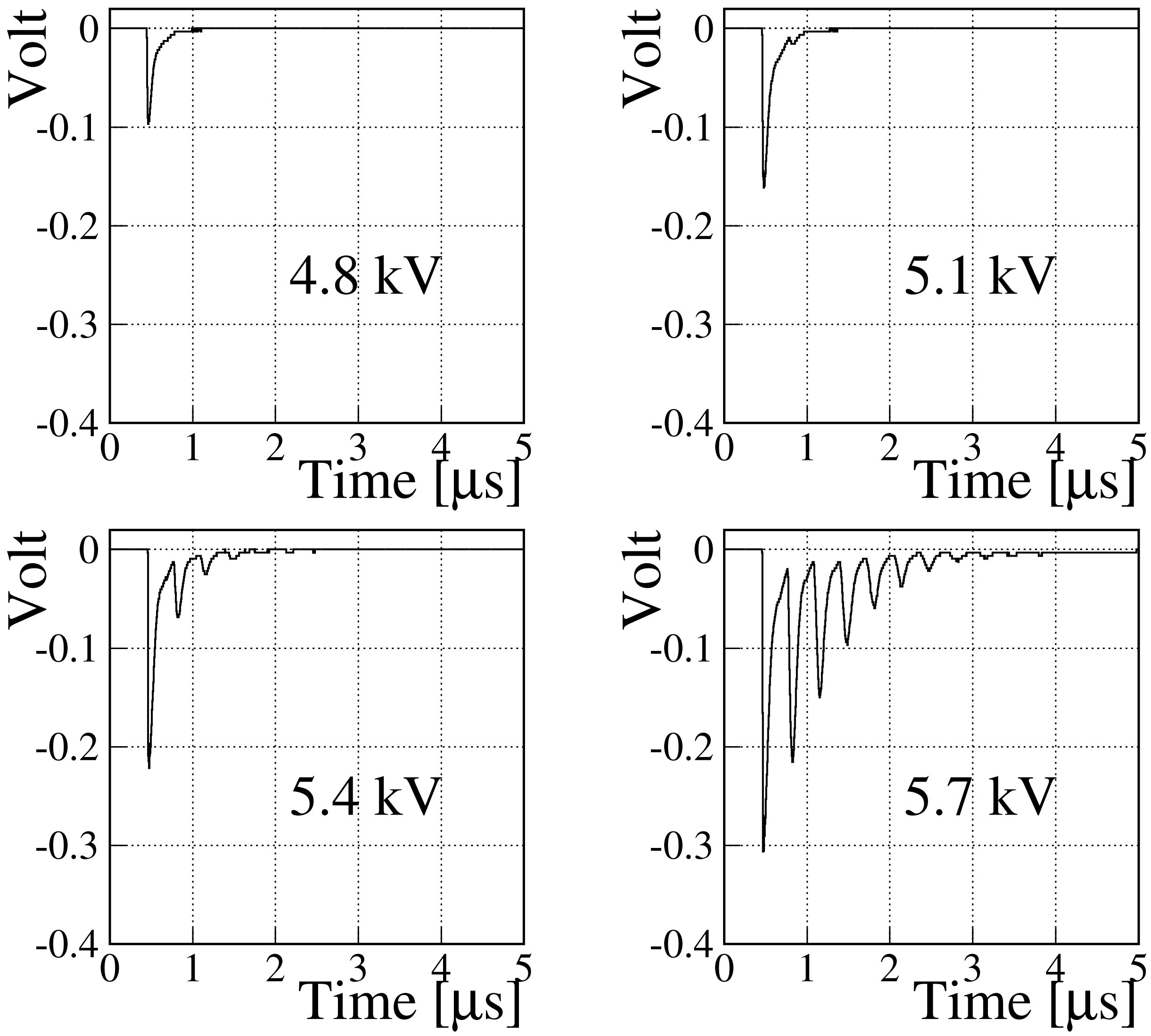

Fig. 5: *Afterpulse probability. The plots were taken at different operating voltages and show the increase in the number of afterpulsing with the HV. The height of the afterpulse peaks is proportional to the fraction of times the first, second, n^{th} afterpulse occurred.*

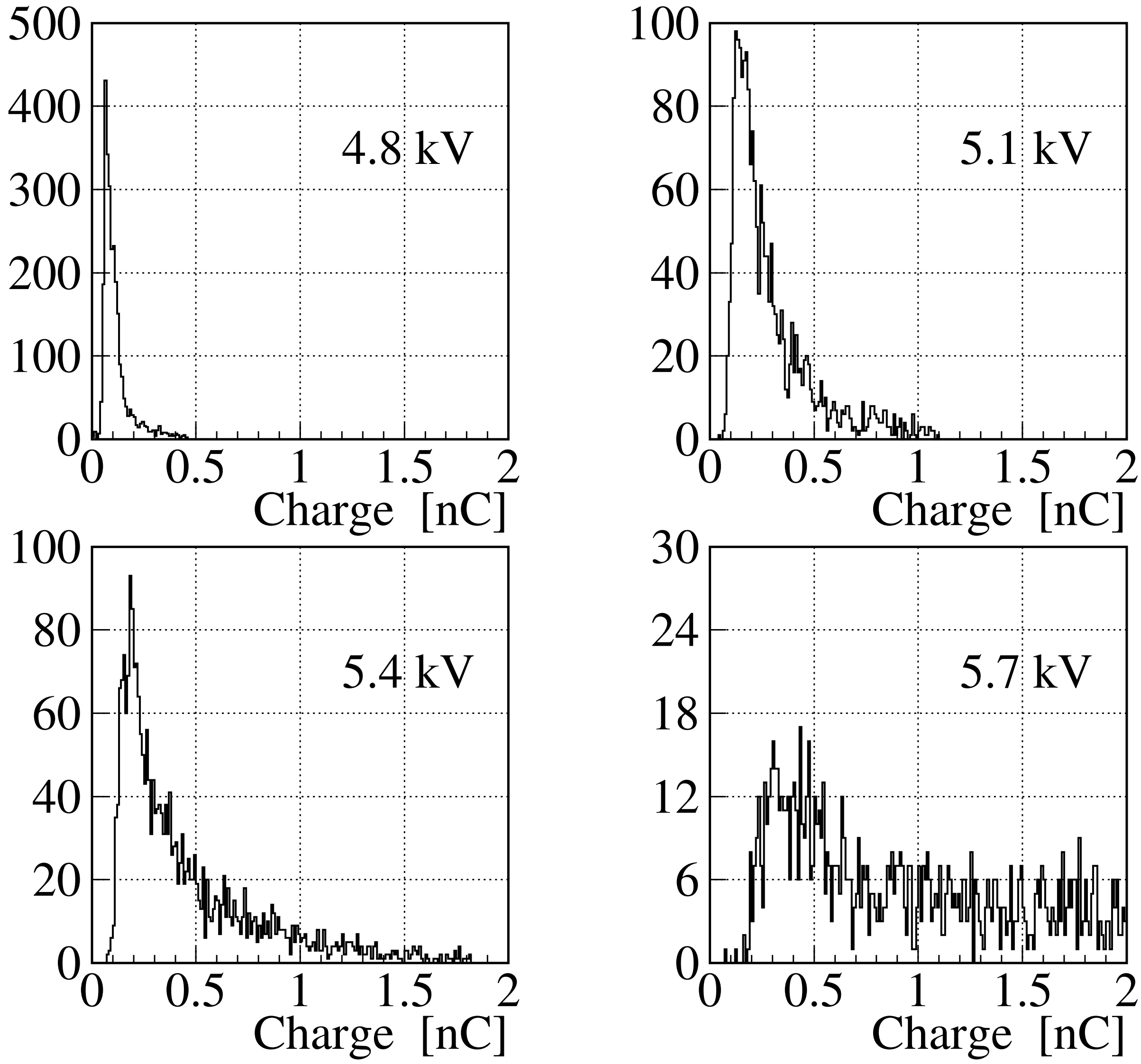

Fig. 6: *Charge spectra for different operating voltages. The average charge of the streamers goes from 100* pC *at 4.8* kV *to 400* pC *at 6.0* kV.

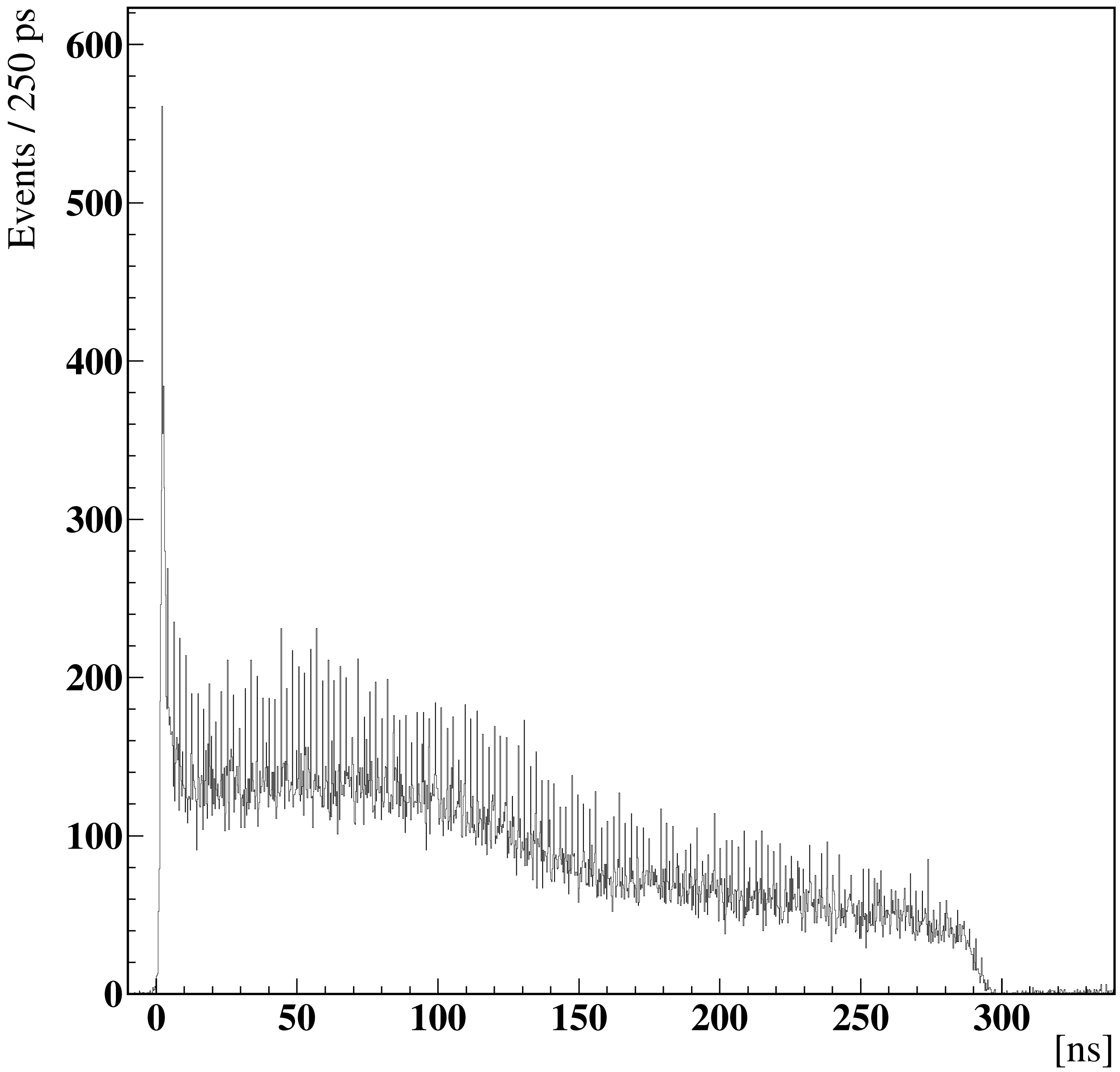

Fig. 7: *Typical drift time spectrum in a tube.*

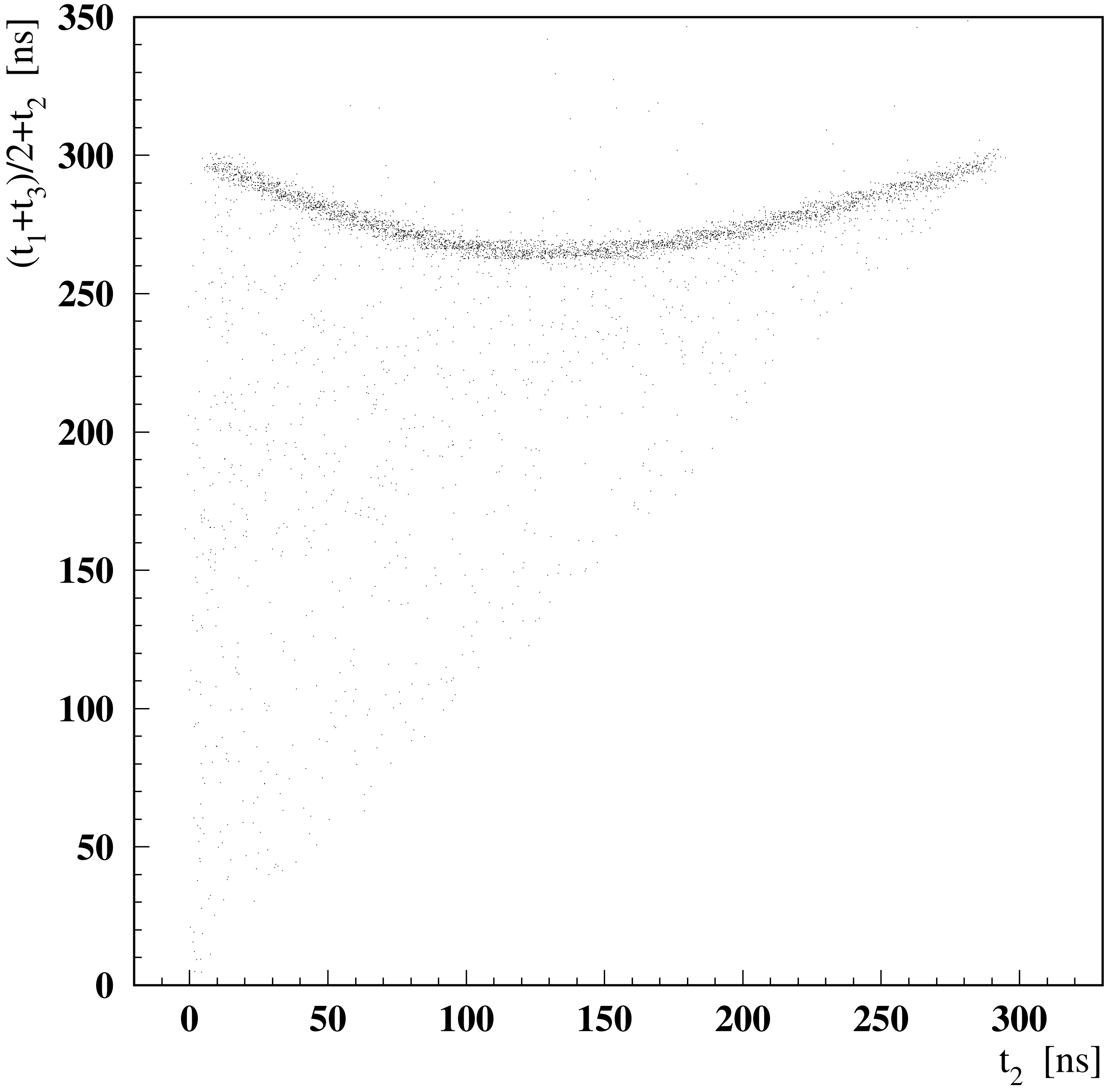

Fig. 8: *Distribution of the function* t_{stag} *defined in the text.*

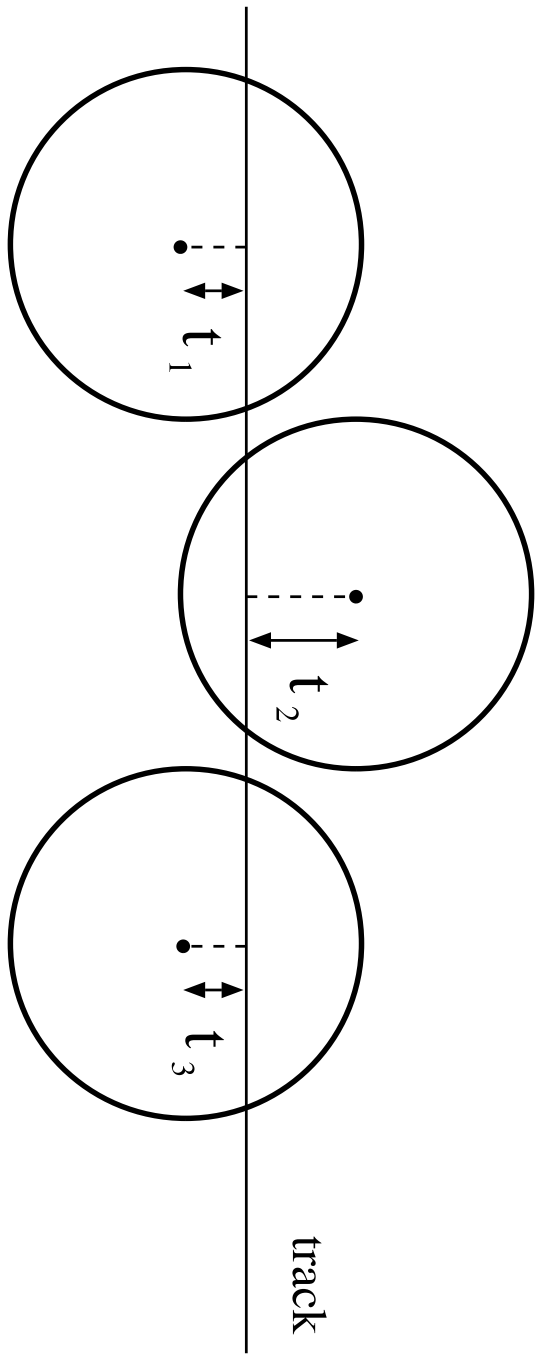

Fig. 9: *Illustration of the symbols related to the* t_{stag} *function.*

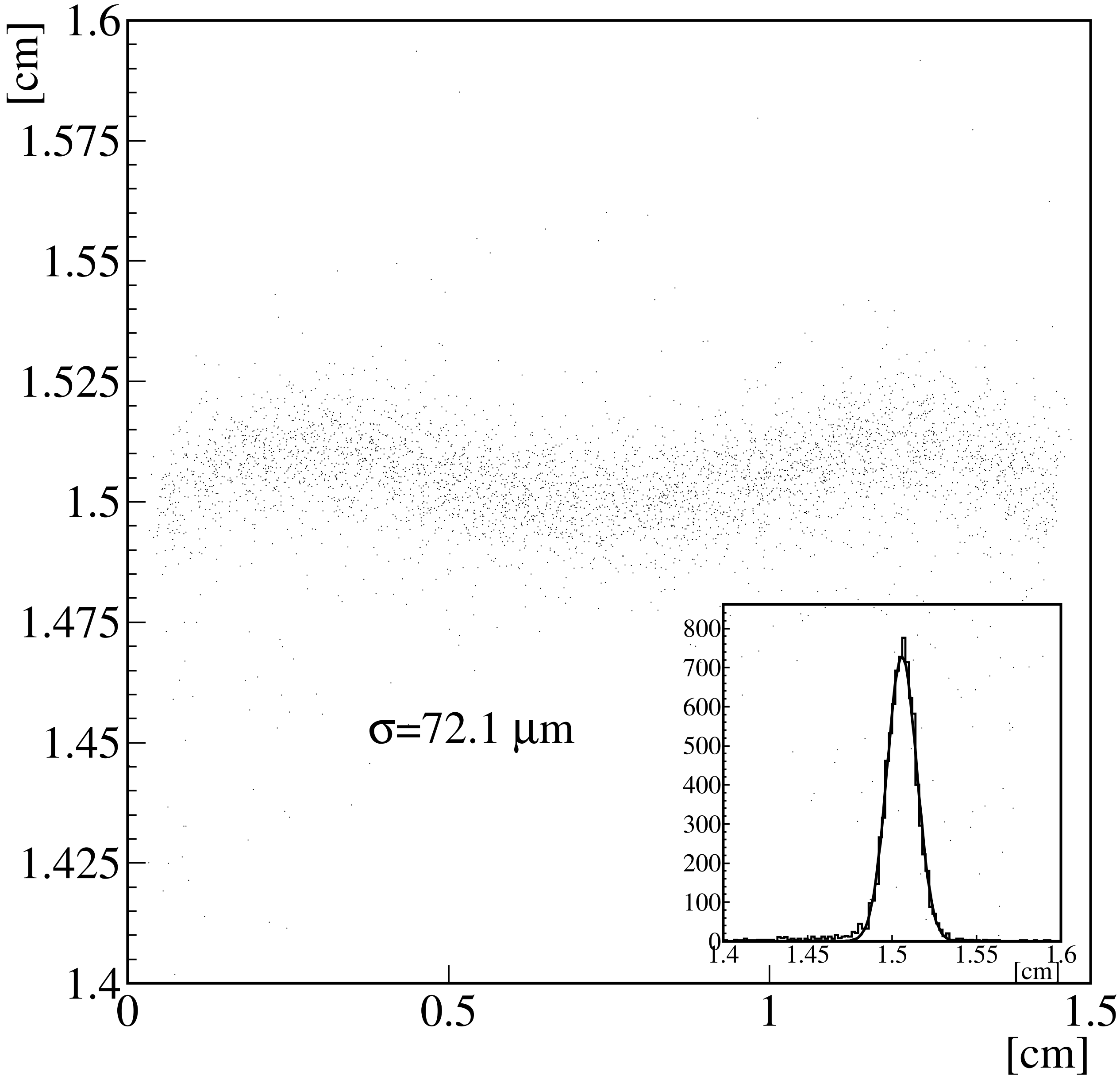

Fig. 10: *Distribution of the function x_{stag} defined in the text. The inset shows the projection of the residuals over the whole tube.*

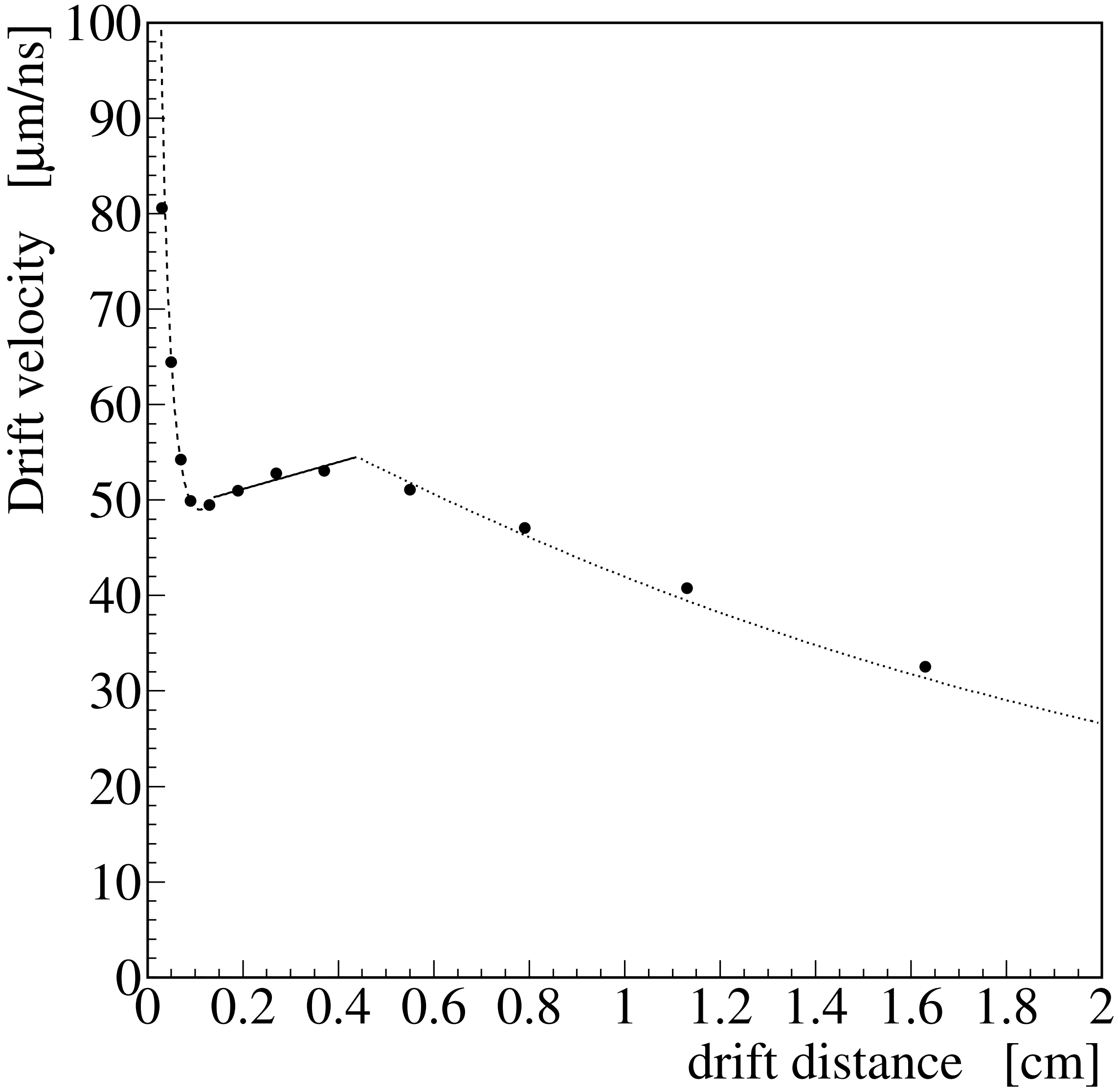

Fig. 11: *Drift velocity in the* $40\%\mathrm{Ar}-60\% i\mathrm{C_4H_{10}}$ *gas mixture used. The points represent the* `MAGBOLTZ` *simulation; they are empirically fitted with the function shown. It has to be stressed that the parabolic approximation is valid only for drift distances greater than* $4 \div 5\,\mathrm{mm}$.

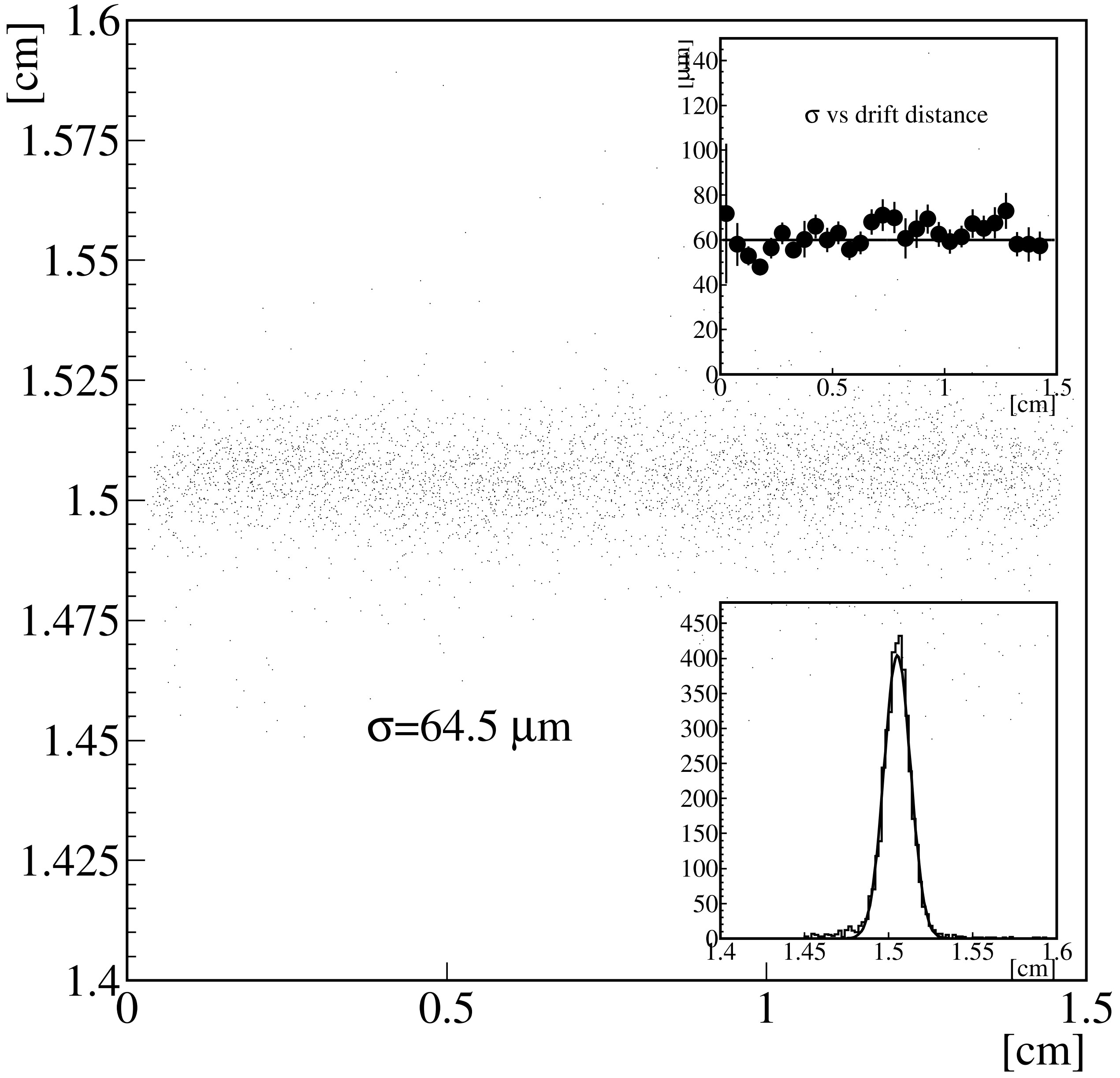

Fig. 12: *Distribution of the function x_{stag} after application of the 'new' space-time relation to the measured drift times. The top inset shows the σ of the distribution as a function of the drift distance, and the bottom one the projection over the whole tube. One can see that indeed most of the systematic effects have been cured.*

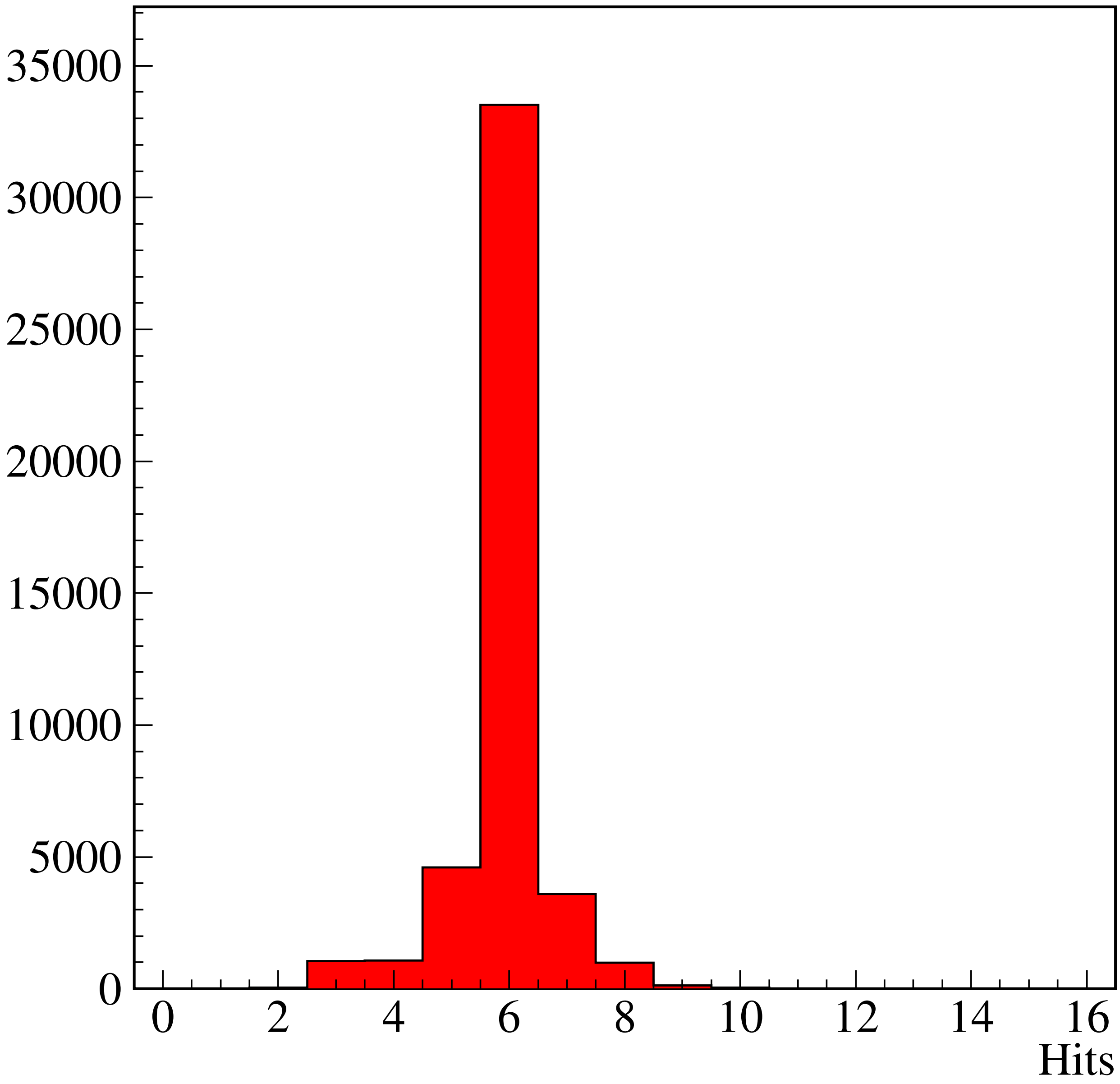

Fig. 13: *Distribution of hit tubes.*

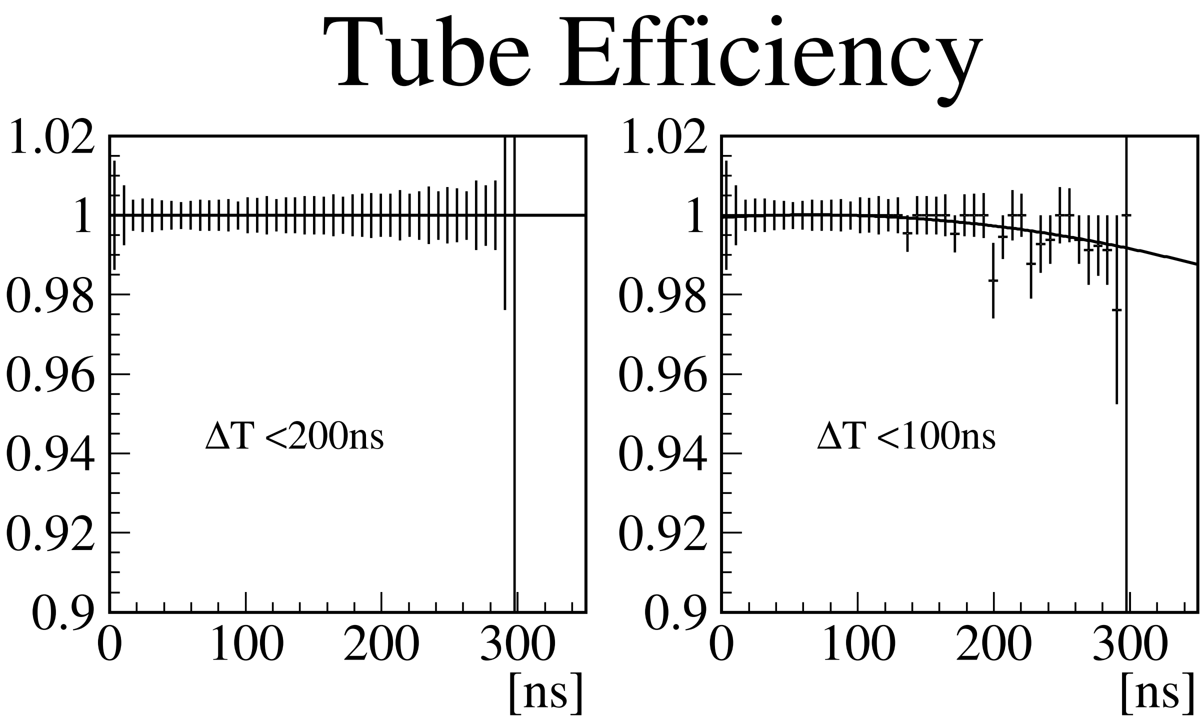

Fig. 14: *Tube efficiency vs. drift time. The efficiency deteriorates at the tube border, but even with the strictest requirement on the agreement between the expected and the measured drift time ($\leq 5\,\mathrm{ns}$) is always $\geq 97.5\%$.*

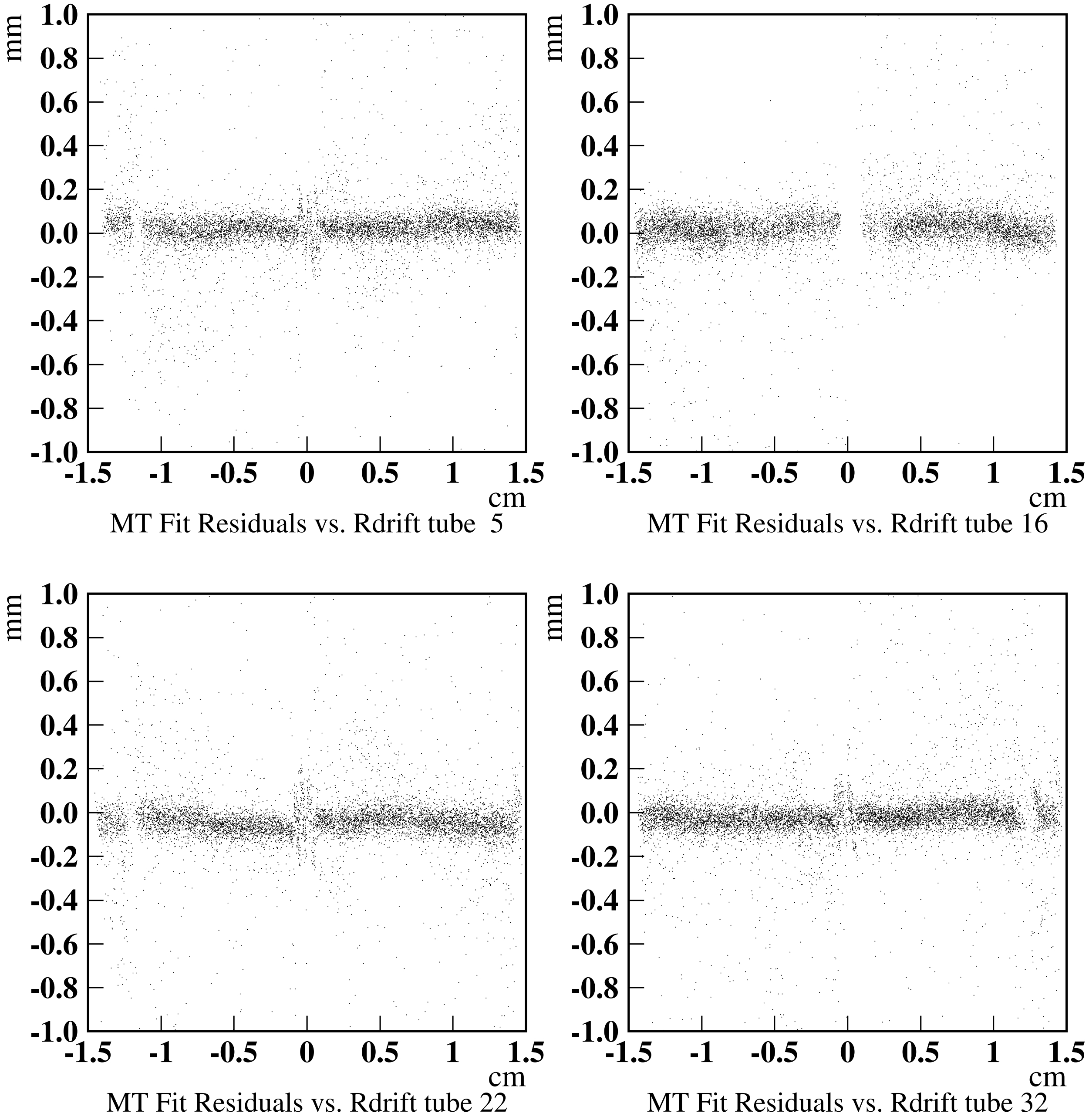

Fig. 15: *Distribution of fit residuals vs. drift distance, for four tubes, each belonging to a different row (see fig. 1).*

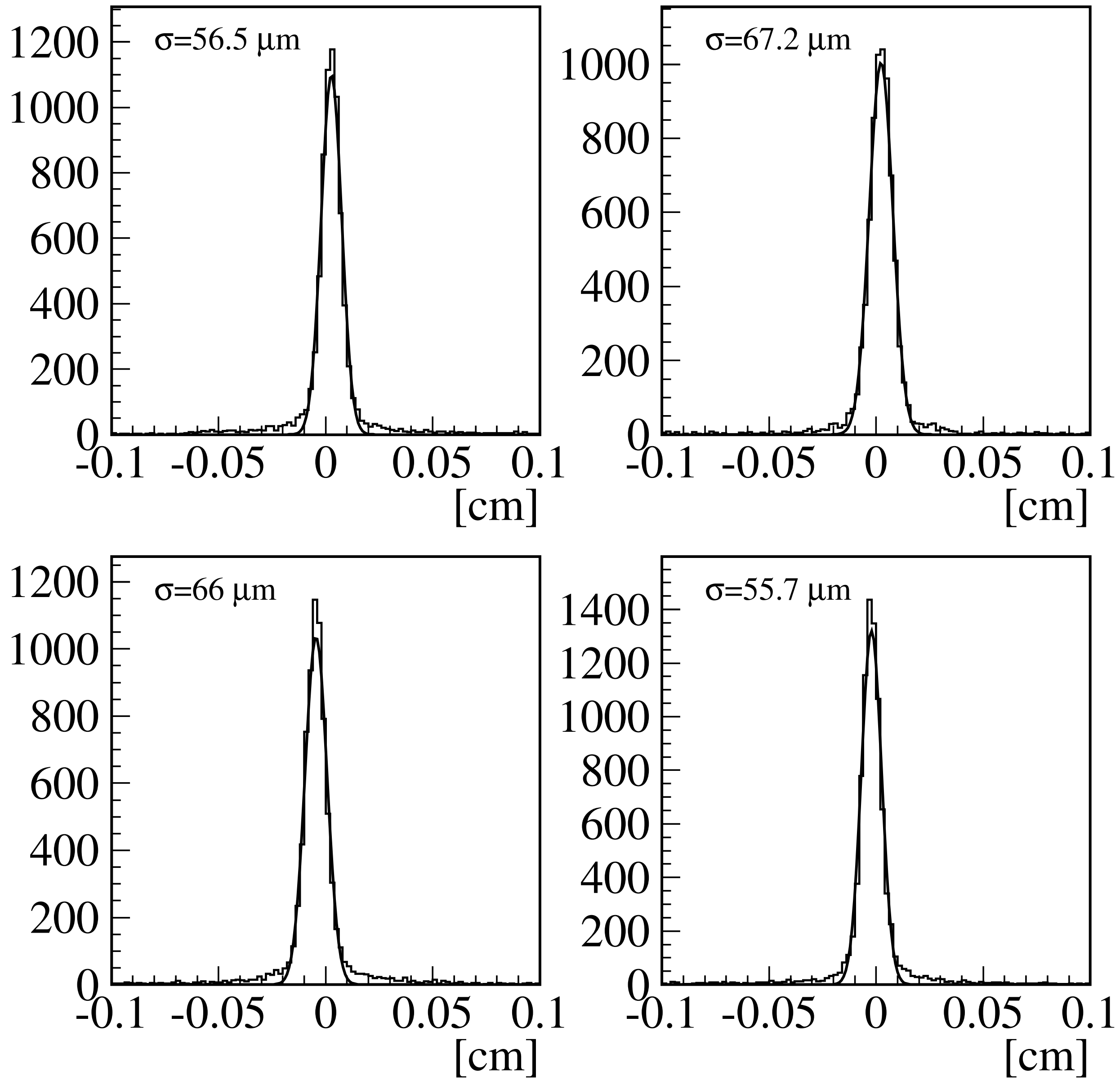

Fig. 16: *Projection of the fit residuals distributions for the four tubes of fig. 15, giving the global resolution of the cells.*

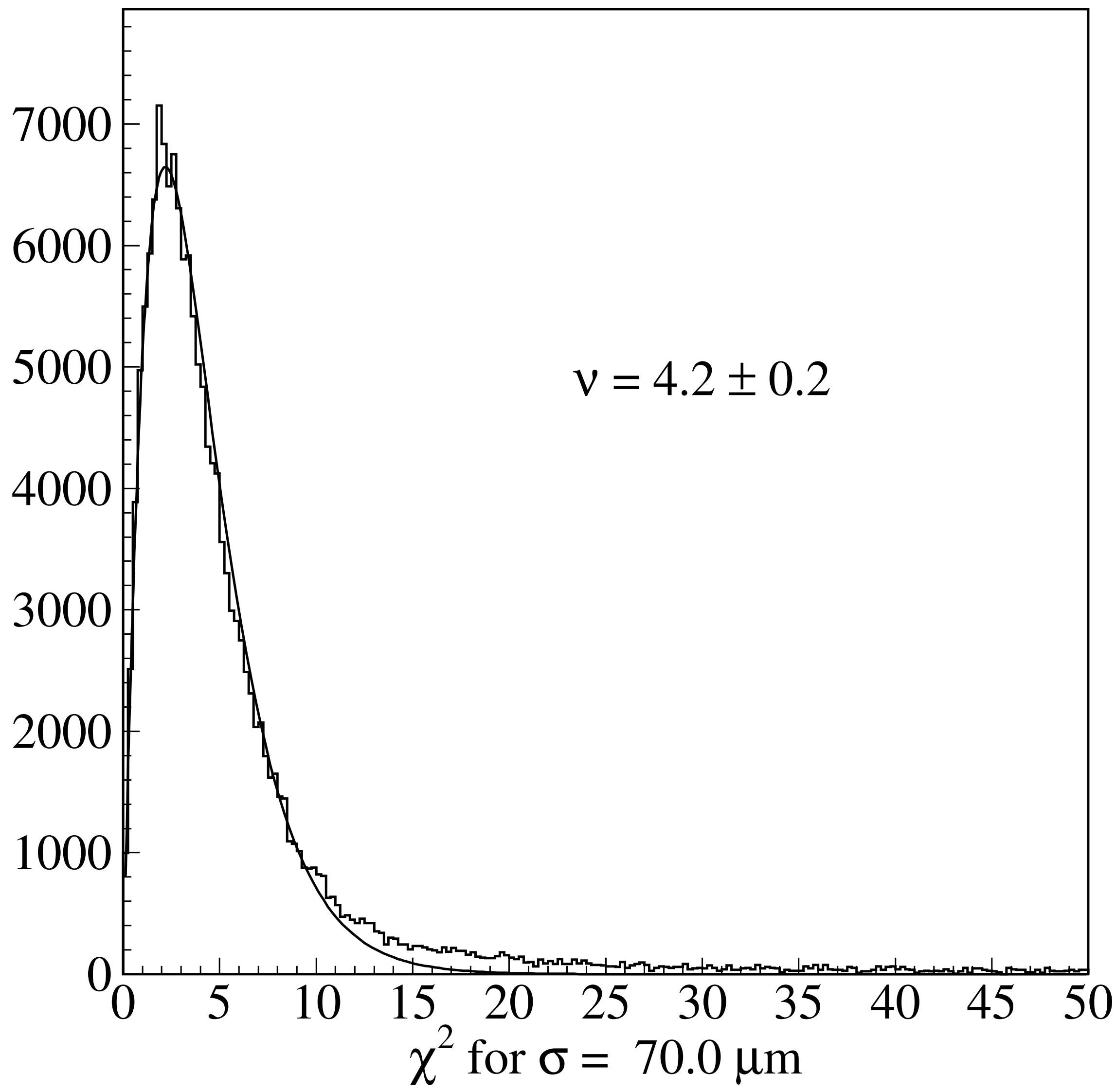

Fig. 17: *Distribution of χ^2 from a straight line fit in the tubes (6 tubes hit). The curve showing a fit to a χ^2 function is superimposed, and the fitted number of d.o.f. is indicated. A 70* μm *error were assigned to the individual measurements.*

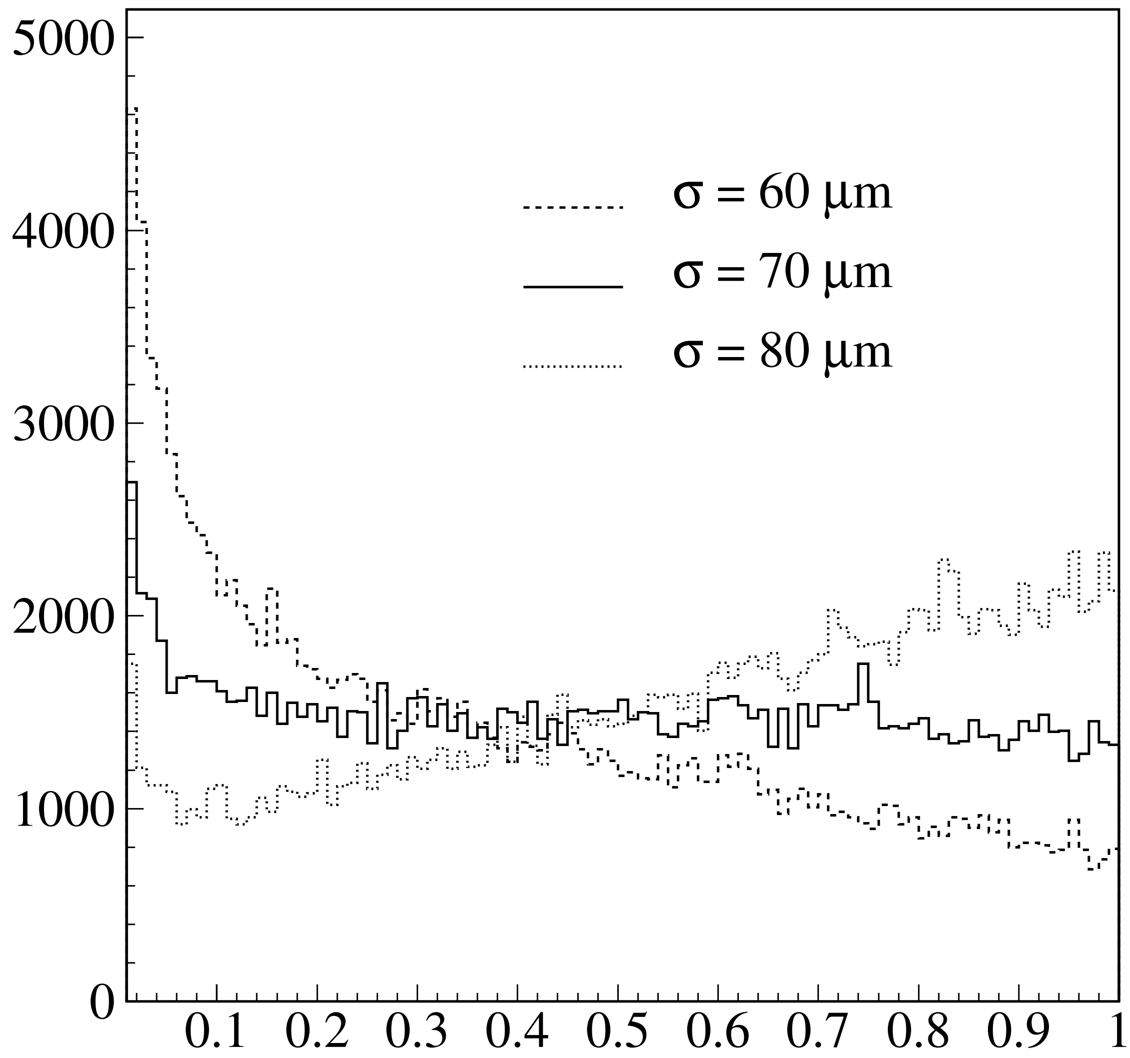

Fig. 18: *χ^2 probability distributions for errors of 60, 70 and 80 μm assigned to the individual tubes, respectively.*

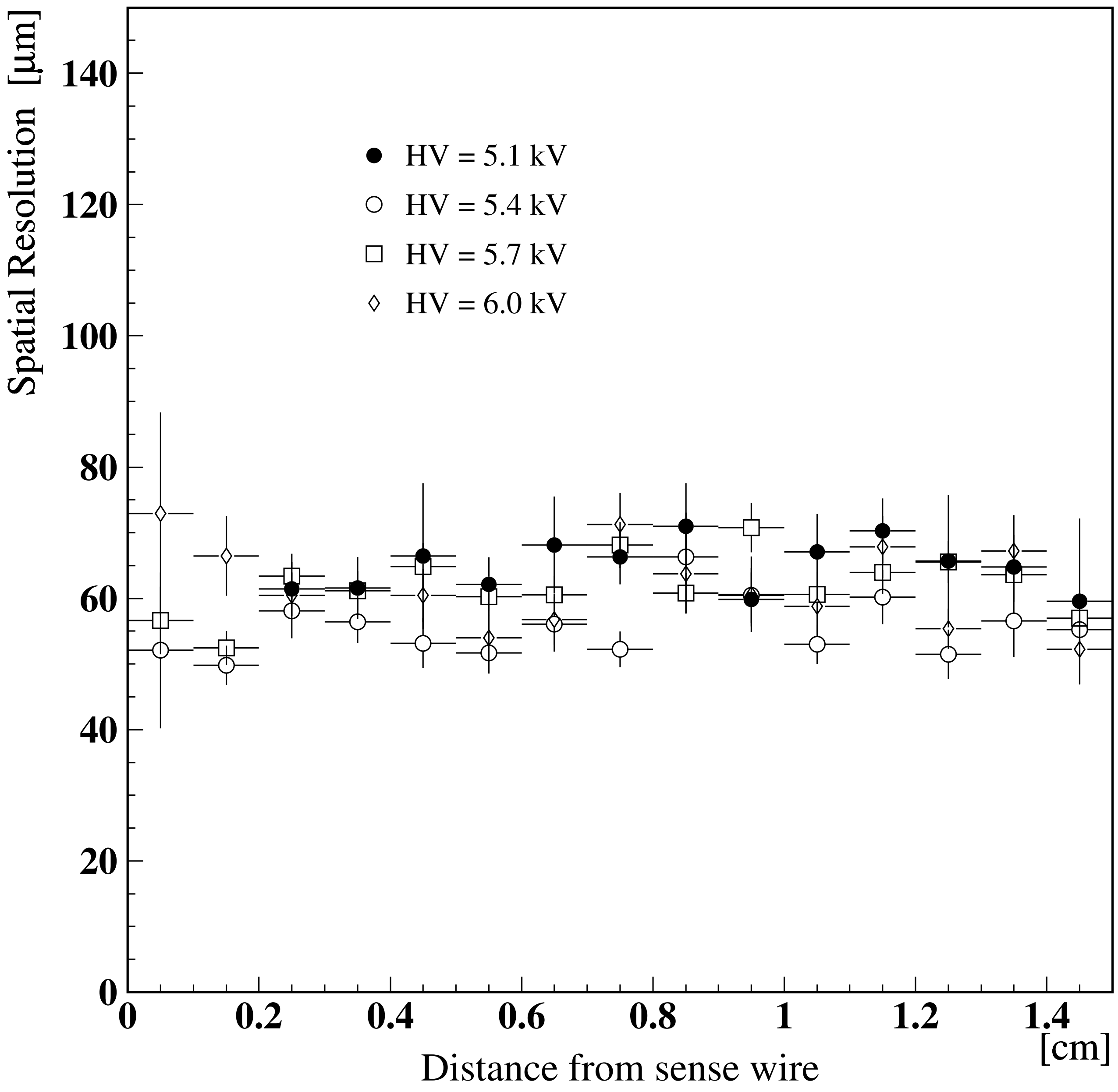

Fig. 19: *Spatial resolution from the x_{stag} ditribution vs. drift distance, for different operating voltages.*

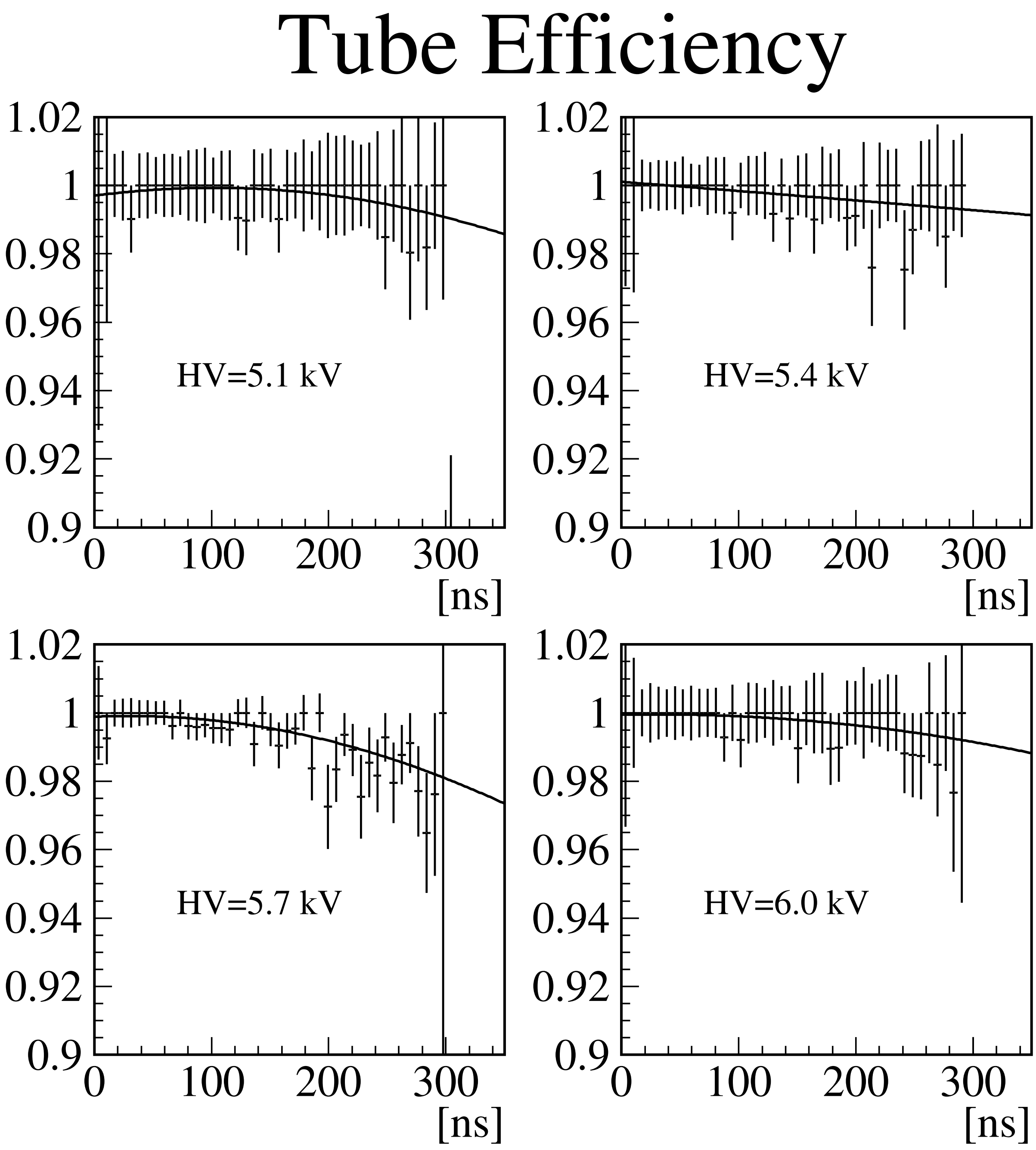

Fig. 20: *Tube efficiency vs. drift time for different high voltage setting. The runs at HV different from 5.7*kV *have poorer statistics; nevertheless, the efficiency is the same within the errors. These plots were obtained cutting at less than 5*ns.

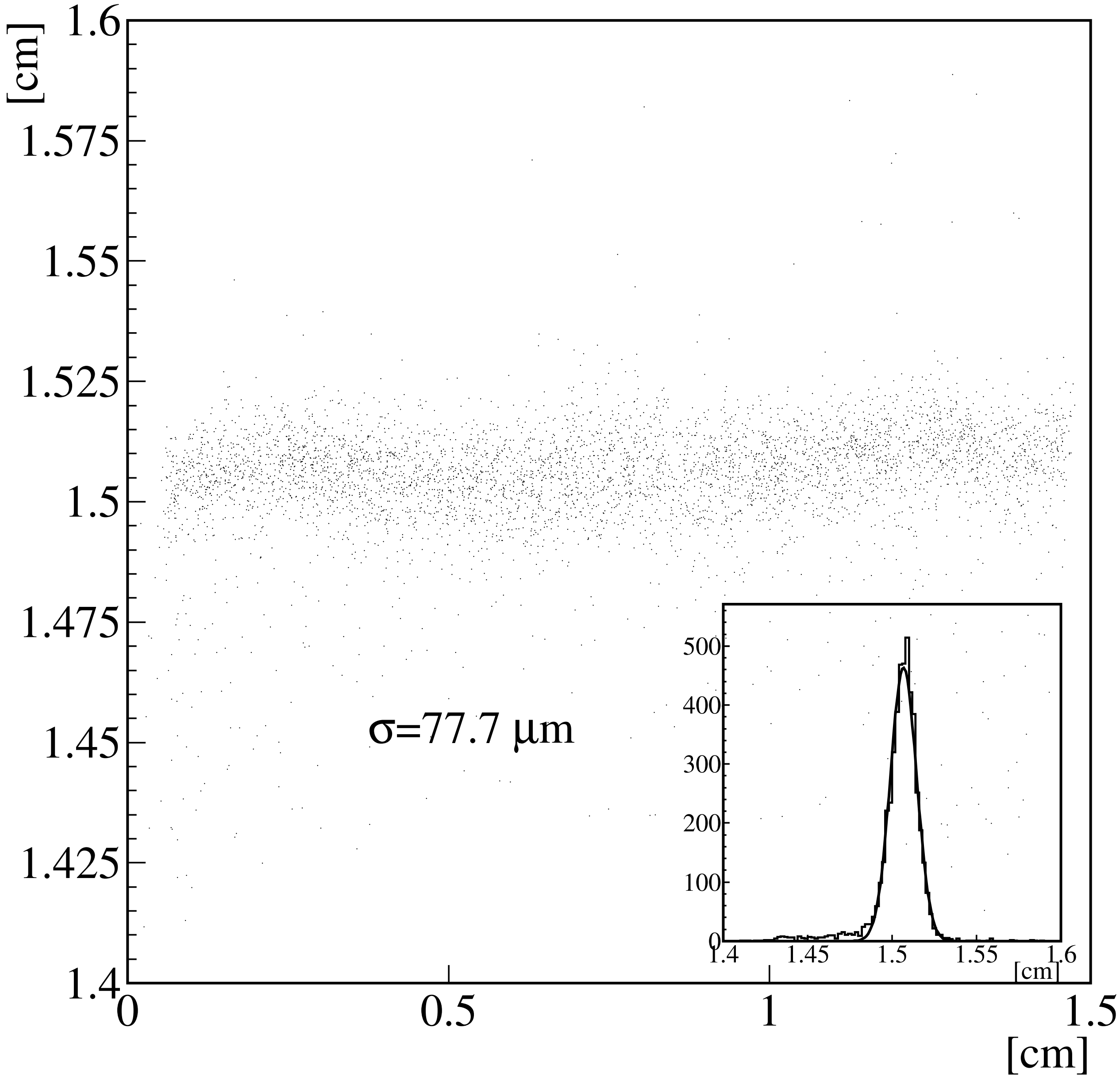

Fig. 21: *Distribution of fit residuals and t_{stag} vs. drift distance, for a tube in magnetic field.*